Periodico di Mineralogia (2011), 80, 1 (Special Issue), 1-17 DOI: 10.2451/2011PM0001

PERIODICO di MINERALOGIA
established in 1930

An International Journal of
MINERALOGY, CRYSTALLOGRAPHY, GEOCHEMISTRY,
ORE DEPOSITS, PETROLOGY, VOLCANOLOGY
and applied topics on *Environment*, *Archeometry* and *Cultural Heritage*

Special Issue in memory of Sergio Lucchesi

Chromite to magnetite transformation: compositional variations and cation distributions (southern Aosta Valley, Western Alps, Italy)

Antonio Della Giusta[1], Susanna Carbonin[1,*] and Umberto Russo[2]

[1]Dipartimento di Geoscienze, Università di Padova, Italy
[2]Dipartimento di Scienze Chimiche, Università di Padova, Italy
[*]Corresponding author: *susanna.carbonin@unipd.it*

Abstract

Massive magnetite bodies in the southern Aosta Valley, NW Italy, are most probably the product of transformation from a chromite proto-ore forming in the ultramafic rocks of an ophiolite suite. Chromium was detected in all the magnetite bodies, except in the Cogne deposit. Chromite-magnetite transformation was examined in spinel samples from the Ussel ore deposit by EMPA, XRD and Mössbauer spectroscopy.

Chemical compositions reveal strong chemical inhomogeneity, mainly for Cr and Fe^{3+}. Spot analyses, from core to rim, in the composite chromite-magnetite grains show significant Al decrease accompanied by Mg and Zn depletion, while the sharp Cr decrease is assisted by Fe^{3+} increase. Cr shows positive linear correlations with Mg, Mn and Zn, and negative with $Fe^{3+}$and Fe^{2+}. Cr/(Cr+Al) (~ 0.75) and Mg/(Mg+Fe^{2+}) (~ 0.15) reveal substantial modifications of the original chromite. At the chromite-magnetite boundary (Cr ~ 0.8 a.f.u.) variations in both major and minor elements are sharp, defining a compositional gap between the normal structure of chromite and the inverse structure of magnetite. At this boundary, Ti^{4+} shows a prominent peak (~ 0.02 a.f.u.) with respect to core and rim, 0.003 and 0.006 a.f.u., respectively. $R^{2+}{}_2TiO_4$ component (R = Fe^{2+}, Mg, Mn^{2+}) is relevant for charge balance requirement and in the transition from chromite to magnetite, due to the inversion of structure.

Single crystal X-ray investigation of seven Cr-magnetites was undertaken to detail intracrystalline cation distributions and to compare them with that of the Cr-free magnetite (Cogne). The non-homogeneity of the chemical composition greatly affects the cell parameters, which do not show any definite trend, in spite of considerable Cr variation. M.a.n. (T) and m.a.n. (M) are almost constant; the only parameter which substantially changes, decreasing Cr, is the oxygen coordinate, from 0.2574 to 0.2553.

The bulk sample from which the seven crystals were selected was also examined by Mössbauer spectroscopy. Its spectrum is typical of magnetite with iron partially replaced by

other divalent and trivalent cations, and consists of two partially overlapping sextets.

Cr is replaced by both Fe^{3+} and Fe^{2+} in the M site, always with a definite disorder of Fe^{2+} in T site. This feature was also observed in the Cogne Cr-free magnetite. All samples retain an average formal iron valence near 2.5^{+} on the M site, suggesting a structure-stabilising role due to charge hopping.

Data suggest that the Cogne magnetite may represent the last stage of the chromite to magnetite transformation, with the sole survival of the inverse spinel structure. Samples from all the other deposits, retaining appreciable amounts of relict Cr-enriched areas, represent a transitional situation, where both normal and inverse structures still coexist. The inhomogeneous chemical composition revealed at the micrometer scale seems to be the consequence of a complex transformation responsible for the survival of microsites the compositions of which recall, but do not fit, those of a chromite proto-ore.

Key words: chromite, magnetite, mineral chemistry, X-ray structure refinement, cation distribution.

Introduction

In a paper concerning the massive magnetite bodies of the southern Aosta Valley, Rossetti et al. (2009) suggested that these ore deposits are most probably the product of transformation from a chromite proto-ore forming in the ultramafic rocks of an ophiolite suite. The chromite to magnetite transformation would have occurred during multiple stages of the complex Alpine metamorphic evolution, including metasomatic exchanges under high fluid activity.

This transformation is recorded by relict Cr-rich micro-areas with compositions trending to that of chromite. These micro-areas are present in all the magnetite bodies excluding that of Cogne. Note that single crystal results for one of these relict micro-areas (sample CROM1 with Cr = 0.1 to 1.4 a.f.u.) have been presented and preliminary discussed in Rossetti et al. (2009).

The aim of the present paper is the crystal chemical characterization of both magnetite and relict Cr-rich spinels, for more information about the chromite to magnetite transformation.

Materials and methods

The magnetite grains chosen for this study come from the Ussel mine, Mount Avic massif (southern Aosta Valley, NW Italy). They belong to LG12, the richest sample in relict cores of chromite (Diella et al., 1994). This is the same source as sample CROM1 studied by Rossetti et al. *(*2009).

Reflected light microscopy

Sample LG12 was crushed and sieved. Several magnetite grains in the ranges 180-250 and 250-355 μm were then polished and examined by reflected light microscopy. The aim was to search for grains with different colours and reflectance indicating chromiferous cores (Figure 1; see also Plate 1 in Diella et al., 1994, and Figure 4 in Rossetti et al., 2009). In the several polished grains examined, the frequency in lower reflectance grey areas, indicating relict chromite, was as high as 70%. Grains with the above features were labelled 1A, 1B, 1C, etc. and some of them were further crushed into fragments (i.e., 1A74 and 1A76; 1C74 and 1C75) in order to obtain crystals suitable for structure refinement.

Figure 1 shows the most common morphologies of the grains. Their strong chemical inhomogeneity is apparent, the grey areas being Cr-rich. In some samples, the inner Cr- portions show relatively sharp borders with the surrounding magnetite. In others, replacement of chromite by magnetite affects the whole grain, so that grey and white areas are randomly distributed throughout the crystal. In sample 4E, not suitable for X-ray analysis, the inner grey area, surrounded by magnetite, has a unique hexagonal morphology with the original crystal faces. Except for this polycrystalline sample, all the other grains shown in Figure 1 were single crystals used for structure refinement.

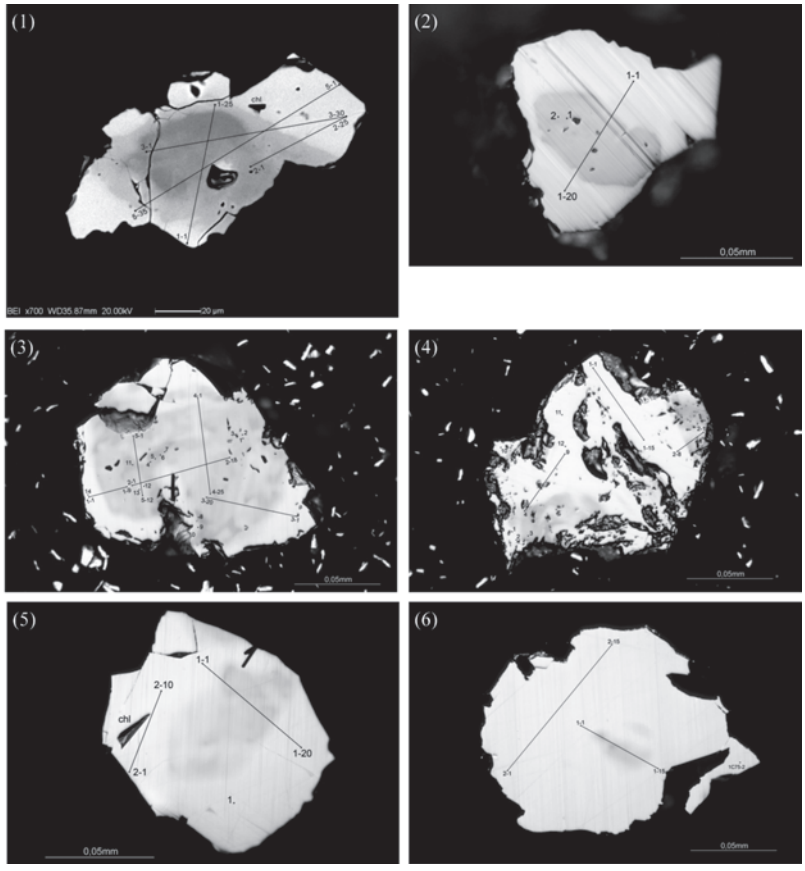

Figure 1. Polished surfaces of some selected crystals and their analytical traverses: (1) CROM1 (back-scattered electron image): dark grey (aluminous) rounded nucleus, surrounded by one or more light grey to white rings; grey areas dominant. In reflected light microscopy: (2) 4E: a unique grey portion (Cr-enriched) with hexagonal symmetry and original crystal faces, surrounded by chromian magnetite; sharp optical boundary; *not a single crystal*. (3) 1A76: diffusive replacement of Cr-spinel by Cr-magnetite affecting the whole grain; grey and white areas distributed throughout crystal (cloudy appearance). (4) 1A74: patchy grey domains in white areas; (5) 1D55; similar to (2) but inner light grey portion (phantom) is also diffusively replaced by Cr-magnetite.(6) 1C75: very small light grey chromiferous core, surrounded by more developed low-Cr magnetite.

Table 1. Average microprobe analyses of samples studied.

	CROM1		1A76		1A74		1D55		3D45		1C74		1B74		1C75	
	wt %	st.dev.	wt %	st.dev.	wt %	st.dev.	wt %	st.dev.	wt %	st.dev.	wt %	st.dev.	wt %	st.dev.	wt %	st.dev.
MgO	1.77	0.91	1.16	0.25	0.89	0.32	0.63	0.12	0.74	0.11	0.66	0.16	0.57	0.15	0.56	0.08
Al_2O_3	4.70	4.53	0.15	0.07	0.11	0.08	0.04	0.03	0.06	0.03	0.05	0.03	0.04	0.02	0.03	0.02
SiO_2	0.11	0.03	0.06	0.07	0.05	0.03	0.08	0.10	0.08	0.03	0.11	0.04	0.05	0.01	0.07	0.03
TiO_2	0.19	0.12	0.47	0.13	0.34	0.19	0.32	0.11	0.28	0.08	0.22	0.11	0.24	0.06	0.20	0.04
Cr_2O_3	32.58	18.93	23.46	9.23	13.55	10.25	9.39	2.92	8.44	1.98	5.37	3.28	6.10	1.98	3.21	1.41
MnO	1.28	0.71	1.12	0.45	0.68	0.55	0.44	0.19	0.41	0.15	0.27	0.24	0.26	0.10	0.16	0.05
FeO	27.87	1.44	28.46	0.75	28.94	1.09	29.78	0.27	29.88	0.27	29.71	0.54	29.91	0.30	30.01	0.32
NiO	0.08	0.08	0.13	0.07	0.12	0.08	0.17	0.09	0.18	0.07	0.16	0.06	0.14	0.02	0.15	0.08
ZnO	0.68	0.49	0.25	0.17	0.12	0.14	0.09	0.09	0.07	0.08	0.07	0.09	0.03	0.02	0.07	0.07
Fe_2O_3	30.41	22.94	44.01	9.54	53.83	10.89	58.61	3.20	60.27	2.04	62.57	3.70	61.98	2.08	65.17	1.59
Sum	99.66		99.27		98.62		99.55		100.40		99.19		99.33		99.63	
cations per 4 O:																
Mg	0.095	0.046	0.065	0.014	0.051	0.018	0.036	0.007	0.042	0.006	0.038	0.009	0.033	0.009	0.032	0.005
Al	0.195	0.186	0.007	0.003	0.005	0.004	0.002	0.001	0.003	0.001	0.002	0.001	0.002	0.001	0.002	0.001
Si	0.004	0.001	0.002	0.003	0.002	0.001	0.003	0.004	0.003	0.001	0.004	0.002	0.002	0.000	0.003	0.001
Ti	0.005	0.004	0.014	0.004	0.010	0.006	0.009	0.003	0.008	0.002	0.006	0.003	0.007	0.002	0.006	0.001
Cr^{3+}	0.925	0.527	0.703	0.273	0.411	0.310	0.284	0.088	0.253	0.058	0.163	0.100	0.186	0.060	0.098	0.043
Mn	0.039	0.022	0.036	0.014	0.022	0.018	0.014	0.006	0.013	0.005	0.009	0.008	0.009	0.003	0.005	0.002
Fe^{2+}	0.855	0.077	0.904	0.028	0.932	0.033	0.954	0.009	0.949	0.010	0.957	0.015	0.962	0.011	0.964	0.006
Ni	0.002	0.002	0.004	0.002	0.004	0.002	0.005	0.003	0.005	0.002	0.005	0.002	0.004	0.001	0.005	0.002
Zn	0.018	0.012	0.007	0.005	0.003	0.004	0.003	0.002	0.002	0.002	0.002	0.003	0.001	0.001	0.002	0.002
Fe^{3+}	0.862	0.674	1.259	0.281	1.561	0.324	1.690	0.095	1.722	0.063	1.813	0.106	1.795	0.063	1.884	0.044
Sum	3.000		3.000		3.000		3.000		3.000		3.000		3.000		3.000	

Electron microprobe analysis

Apart from the samples shown in Figure1, several grains with evident chromiferous cores were also selected for chemical investigation, although they were not suitable for X-ray analysis, not being single crystals (e.g., sample 4E in Figure 1). Single crystals used for structure refinement (five from Figure 1, plus three others, 3D45, 1B74 and 1C74; Table 1) were polished and chemically analysed after X-ray data collection.

Analyses were performed with a CAMECA SX50 electron microprobe fitted with four wavelength-dispersive spectrometers and one energy-dispersive spectrometer at the CNR-IGG, Padova. Operating conditions were: accelerating voltage 15 kV, sample current 15 nA, count times 10 s on peaks and 5 s on backgrounds. X-ray counts were converted into oxide weight percentages by a PAP correction program provided by CAMECA. Synthetic oxide and natural mineral standards were used, and results were monitored against the same standards. Analyses were carried out after a check that I_{Xstd}/I_{std} was 1.00 ± 0.01 for each element, where I_{Xstd} was the intensity of the analysed standard and I_{std} the intensity of the same standard monitored after each element calibration.

Points analysed at the microprobe are from hundreds to tens, depending on crystal size and number of selected traverses from core to rim. Fe^{3+} was calculated on the basis of stoichiometry, i.e., three cations per four oxygens. Average analyses are listed in Table 1 (spot analyses and analytical traverses are available from the authors upon request). Standard deviations, mainly those for major elements involved in the transformation from chromite to magnetite, were very large, and mainly affected determination of cell parameters, as will be shown below.

Table 2. Conditions of X-ray data collection for a typical experiment (sample 1A74).

Radiation	Mo*K*α (0.71073 Å)
Monochromator	High crystallinity graphite crystal
Collimator (mm)	0.5
2θ range (°)	6.9 - 95.6
Reciprocal space range	-16,-9,-16≤ h, k, l ≤13,17,8
Reflections collected	7051
Scan method	ω
Scan speed (°/s)	0.04

Single crystal X-ray diffraction

X-ray diffraction data were collected at the Department of Earth Sciences, University of Padova, on the seven new crystals listed in Table 1 (from 1A76 to 1C75), all selected from sample LG12 (Ussel). In order to distinguish them from and compare them with 'chromite' and magnetites, they are henceforth called Cr-magnetites.

Intensity diffraction data were collected in the conditions listed in Table 2 on a Stadi4 CCD diffractometer operating at 50 kV and 40 mA, and equipped with an area detector. After data collection, intensities were corrected for Lorentz and polarization factors, and the absorption correction calculated using optimised shape (X-SHAPE, STOE 1999). Structural refinements were carried out against Fo^2 in space group $Fd\bar{3}m$ (with origin at $\bar{3}m$) with the SHELX97 program (Sheldrick, 1997). No chemical constraints were imposed on the refinements. Only the Fe scattering curve, not constrained to full site occupancy, was used for both tetrahedral and octahedral sites. Refinements showed the strong dependence of site occupancies on the ionisation level of oxygen, as discussed in Della Giusta et al. (1986). Following the procedure described in Salviulo et al. (2000), neutral cations and partially ionised oxygen were found to be the most suitable to obtain the best value for all

Table 3. Results of cell parameter measurements and structural refinements.

	1A76	1A74	1D55	3D45	1C74	1B74	1C75
dimensions (μm)	175·100·75	150·100·75	150·100·80	100·100·50	150·100·75	100·75·75	150·150·80
a (Å) (1)	8.398 (8)	8.397 (4)	8.400 (2)	8.397 (3)	8.40 (1)	8.397 (3)	8.393 (4)
a (Å) (2)	8.3981 (7)		8.3953 (2)			8.3945 (2)	
u	0.2574 (4)	0.2563 (2)	0.2555 (2)	0.2554 (1)	0.2556 (1)	0.2556 (1)	0.2553 (1)
M-O (Å)	2.040 (3)	2.048 (2)	2.055 (2)	2.055 (1)	2.0543 (3)	2.053 (1)	2.055 (2)
T-O (Å)	1.925 (5)	1.909 (3)	1.899 (3)	1.897 (2)	1.900 (3)	1.900 (2)	1.894 (2)
$R_{4\sigma}$	0.050	0.025	0.028	0.018	0.018	0.017	0.019
R_{all}	0.077	0.042	0.057	0.044	0.040	0.044	0.039
wR2	0.140	0.050	0.055	0.029	0.031	0.034	0.034
Goof	0.983	0.963	0.860	0.772	0.783	0.791	0.857
$N_{4\sigma}$	107	114	113	106	110	111	115
N_{all}	159	158	166	151	154	156	156
Ext. coeff.	0.00000	0.0016 (4)	0.0009 (3)	0.0020 (2)	0.0021 (2)	0.0017 (2)	0.0046 (3)
U_{eq} (Ox) (Å^2)	0.0109 (9)	0.0089 (4)	0.0096 (5)	0.0073 (3)	0.0079 (3)	0.0082 (4)	0.0085 (3)
U_{eq} (M) (Å^2)	0.0114 (3)	0.0092(1)	0.0102 (2)	0.0081 (1)	0.0085 (1)	0.0083 (1)	0.0090 (1)
U_{eq} (T) (Å^2)	0.0116 (4)	0.0084 (2)	0.0089 (2)	0.0067 (2)	0.0073 (2)	0.0072 (2)	0.0075 (2)
m.a.n. (T)	26.6 (7)	25.8 (2)	26.0 (2)	26.2 (1)	26.2 (2)	26.3 (2)	26.2 (2)
m.a.n. (M)	25.2 (6)	25.2 (2)	25.4 (2)	25.5 (1)	25.4 (1)	25.5 (1)	25.7 (1)

(1) area detector; (2) point detector; $R_{4\sigma}$: disagreement factor for reflections with I >4σ(I); wR2: weighted disagreement factor and Goof: Goodness of fit (Sheldrick, 1997); Ext. Coeff.*:* secondary extinction coefficient; *U*eq: isotropic displacement parameters; m.a.n.: mean atomic numbers in considered sites.

conventional agreement factors. An ionisation level between 50% and 75% was adopted for the oxygen scattering curve.

The refined parameters were scale factors, secondary extinction coefficient in all but one sample, oxygen coordinate *u,* tetrahedral and octahedral site occupancies, and isotropic displacement parameters *U*. Results of structural refinements of Cr-magnetites are listed in Table 3 (ordered according to decreasing Cr content). Refined site occupancies are expressed as mean atomic numbers m.a.n. (T) and m.a.n. (M) in T and M sites, respectively. Agreement factors improve with decreasing Cr content of the crystal. The mean m.a.n. (T) value, 26.2(2), clearly indicates that Fe atoms are dominant in the T site. Instead, the mean m.a.n. (M) value is lower, 25.4(2), indicating substitutions by lighter elements than Fe. M.a.n. (T) and m.a.n. (M) are almost constant; the only parameter which decreases with Cr content is the oxygen coordinate, from 0.2574 to 0.2553.

Cell parameter measurements

Lattice parameters were first measured on the Stadi4 CCD diffractometer, equipped with an area detector, in the 2θ range 6.8-50°, and between 450 and 820 reflections were used. Diffractometer alignment was checked by measuring the cell parameters of a stoichiometric pure spinel and a quartz crystal. As Table 3 and Figure 2 show, the precision is not high, as the estimated standard deviations of the cell dimension measurements are a few units on the third and in one case on the second decimal digit. The considerable non-homogeneity in the composition of the crystals undoubtedly had a dramatic effect on crystal structure, primarily on cell dimensions. In spite of this, the studied samples are still single crystals suitable for X-ray data collection.

Note that, as Cr content increases, so does its standard deviation (Table 1). This chemical feature was found to be correlated with typical half-widths of the X-ray reflections. Initial analysis was performed on CROM1 with a STOE AED4 four-circle diffractometer, with a graphite monochromator for Mo*K*α radiation, operating at 50 kV and 40 mA. Diffraction profiles of reflections used for unit-cell determination (Rossetti et al., 2009) were quite broad, and typical half-widths were ~ 0.75° in ω. Similar features appeared on three of the new Cr-magnetites studied here, according to the procedure described below. In order of decreasing Cr content, they were: 1A76 (Cr = 0.70(27) a.f.u.), 1D55 (Cr = 0.28(9) a.f.u.), and 1B74 (Cr = 0.19(6) a.f.u.). Typical half-widths of reflections were between 0.21(1) and 0.6(1)° in ω for the first sample, between 0.164(3) and 0.30(4)° in ω for the second, and between 0.101(5) and 0.136(6)° in ω for the third.

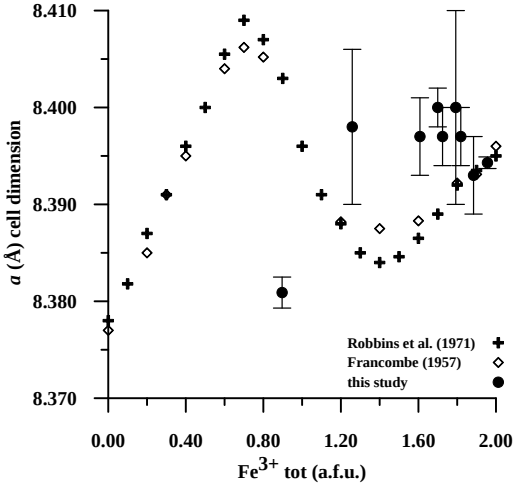

Figure 2. Plot of lattice parameter (*a*) measurements against Fe^{3+} tot (a.f.u.) in Cr-magnetites: despite great variations in Fe^{3+} content, they show no definite trend. Only one filled circle, plotting far from the others, is CROM1(*a* = 8.3809 Å; Rossetti et al., 2009): small *a* value is due to smaller cations in T and M sites with respect to Cr-magnetites. Also plotted are data of Robbins et al. (1971) and Francombe (1957): for comments, see text.

These three crystals were chosen to test determination of unit-cell parameters also by means of a four-circle diffractometer equipped with an unfiltered Mo sealed-tube X-ray source without monochromator (Angel et al., 1997). X-ray data collection was performed on a STOE STADI IV operating at 50 kV and 40 mA and controlled by SINGLE software (Angel et al., 2000). This diffractometer was optimised for measurement of unit-cell parameters, following the recommendations of Angel et al. (2000). Accurate centering of the crystal under the X-ray beam was achieved by iterative adjustment of the crystal offset calculated by the software. During the centering procedure, the effects of crystal offsets and diffractometer aberrations were eliminated from the refined peak positions by the eight-position centering method of King and Finger (1979). Unconstrained unit-cell parameters were obtained by vector least-squares (Ralph and Finger, 1982). The symmetry-constrained unit-cell parameters listed in Table 3 were found to be within one estimated standard deviation of the unconstrained ones.

Table 3 and Figure 2 show that the cell parameters of the seven Cr-magnetites do not show any definite trend, in spite of the great variations in Cr - Fe^{3+} contents. In addition, two of the determinations with the point detector [Cr-magnetites 1B74: *a* = 8.3945(2) Å; 1D55: *a* = 8.3953(2) Å] give cell parameters smaller than those determined with the area detector, and very close to that of pure magnetite [8.3949 Å, Nakagiri et al., 1986; Della Giusta et al., 1987]. The higher value of the third determination (1A76, Table 3), very close to that found with the area detector [8.3981(7) Å], may be due to maximum Fe^{2+} in the T site and also to higher Mn^{2+} content (Table 4).

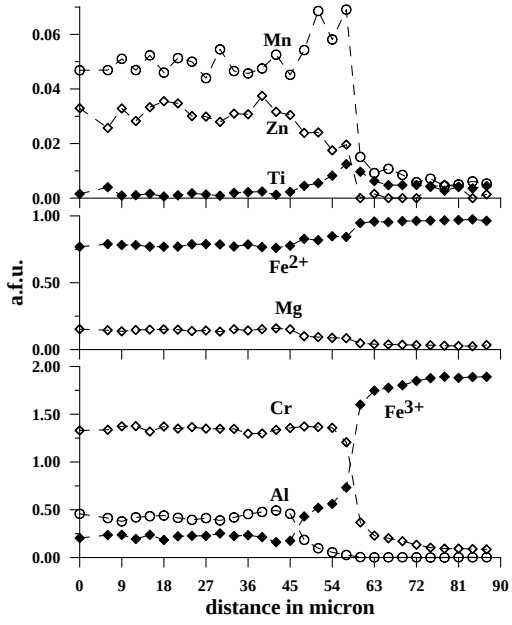

Figure 3. Results of electron microprobe analytical traverse 3 in sample CROM1 from dark grey core, across light grey, to white rim (see Figure 1).

Mössbauer spectroscopy

Bulk sample LG12, from which all the seven new crystals were separated, was also studied by Mössbauer spectroscopy at the Department of Chemical Sciences, University of Padova. Measurements were performed on a conventional constant acceleration spectrometer equipped with a room-temperature Rh matrix ^{57}Co source. All spectra were collected at room temperature (RT). Hyperfine parameter isomer shift (IS), quadrupole splitting (QS) and full linewidth at half-maximum (Γ), expressed in mm s^{-1}, were obtained by means of a standard least-squares minimisation technique. The spectra were fitted to Lorentzian line shapes with a minimum number of doublets. The IS is quoted relative to metallic iron at room temperature.

Results

Mineral chemistry

As an example of the compositional variations from chromite to magnetite, we consider analytical traverse 3 in CROM1 (Figure 1) (new analyses, not reported in Rossetti et al., 2009), because its chemistry spans the compositions of all the other grains studied. Figure 3 plots atoms per formula unit (a.f.u.) from the darkest grey core, across light grey, and lastly to the white rim of the crystal; between about 45 and 54 μm (from dark to light grey) Al decreases virtually to zero, accompanied by Mg and Zn depletion. Atomic ratios Cr/(Cr+Al) and Mg/(Mg+Fe^{2+}) for the dark grey core (between 0.73 and 0.78, and 0.17 and 0.15, respectively) reveal substantial modifications of the original chromite, as also reported by Diella et al. (1994) and Rossetti et al. (2009). At about 57 μm of the traverse (from light grey to white), the change from Cr-spinel to magnetite is marked by a sharp decrease in Cr^{3+} and an increase in Fe^{3+}. Note that at this boundary Ti^{4+} shows a prominent peak with maximum content (~ 0.02 a.f.u.) with respect to the core, where it is minimum (~ 0.003 a.f.u.), and the rim where it occurs in small quantities (~ 0.006 a.f.u.). Mn^{2+} also shows a slight although more scattered increase here, with respect to the content of the innermost part. In Figure 3, in spite of the relatively wide microprobe beam (about 3 μm), the sharp variations of both major and minor elements at the chromite-magnetite boundary clearly define the compositional gap between the normal structure of residual chromite and the inverse structure of Cr-poor magnetite.

Figure 4 shows the positive linear correlations of Cr^{3+} (a.f.u.) with Mg, Mn and Zn, and negative ones with Fe^{3+} and Fe^{2+}. These correlations are less distinct at high Cr contents, mainly due to the fast but discontinuous depletion of Al. The striking feature is the non-linear correlation of Ti^{4+} with all other elements,

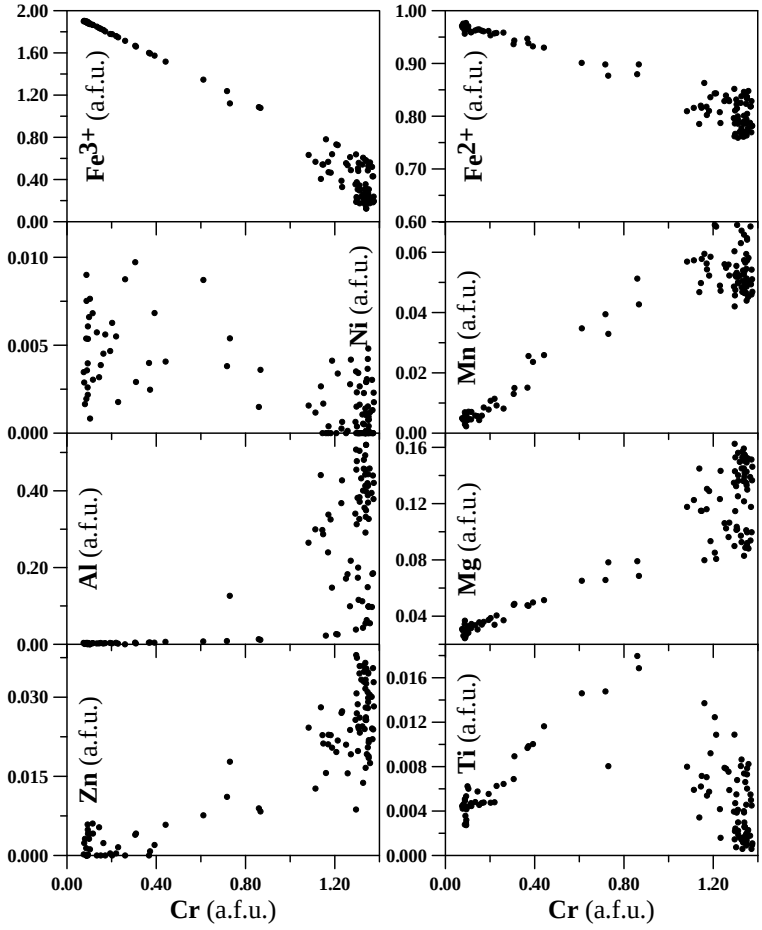

Figure 4. Plots of Cr vs. Fe^{2+}, Fe^{3+}, Ni^{2+}, Mn^{2+}, Al, Mg, Zn and Ti^{4+} in CROM1 (all analyses).

instead its bell-shaped distribution, as shown in Figure 5. Due to this unique distribution, we tentatively calculate spinel composition at maximum Ti^{4+} content as follows:

$$(Fe^{3+}_{1.18}\ Fe^{2+}_{0.90}\ Cr^{3+}_{0.77}\ Mg_{0.07}\ Mn^{2+}_{0.05}\ Ti^{4+}_{0.02}\ Al_{0.01})\ O_4.$$

Thus, maximum Ti^{4+} content occurs precisely at the boundary between chromite and magnetite (Beeson and Jackson, 1969; Onyeagocha, 1974; Loferski and Lipin, 1983; Zakrzevski, 1989; Diella et al., 1994; Barnes, 2000; Mellini et al., 2005; Fontana et al., 2008). Barnes attributed it to 'relatively slow rate diffusion for Ti in magnetite'.

We emphasize that: (1) $R^{2+}_2TiO_4$ component contributes to the charge balance requirement, due to the definite decrease in Al (i.e., $2Al^{3+} = R^{2+} + Ti^{4+}$ with R = Fe^{2+}, Mg, Mn^{2+}) as Cr decreases to ~ 0.8 a.f.u.; this component then diminishes again towards magnetite; (2) due to the strong octahedral preference of Ti^{4+} and the inverse

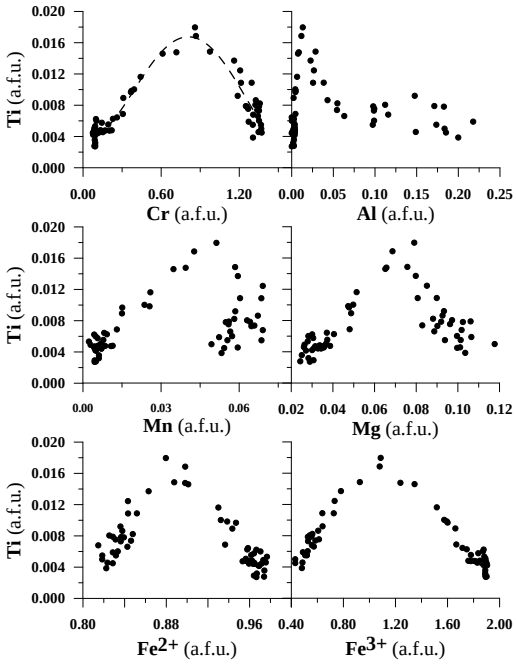

Figure 5. Plots of Ti^{4+} vs. major elements in CROM1. Only analyses yielding Cr/(Cr+Al) ≥ 0.85 are plotted (*i.e.,* from light grey to white rim; see Figure 1). Dashed curve: 4th-order polynomial best fit.

structure of $R^{2+}{}_2TiO_4$, the role of Ti^{4+} on the transition from chromite to magnetite also favours the transition from normal to inverse structure.

Cation distribution

A sufficiently reliable intracrystalline cation distribution was obtained with the procedure described by Lavina et al. (2002), minimising the following function:

$$F(X_i) = 1/n\ \Sigma_j\{[O_j - C_j(X_i)]/\sigma_j\}^2$$

where X_i are site atomic fractions of the i^{th} cation and O_j are observed quantities with their standard deviations σ_j. O_j are the four observed crystallographic parameters, i.e., cell parameter *a*, oxygen coordinate *u,* m.a.n. (T) and m.a.n. (M), plus the chemical proportions for a total of n. $C_j(X_i)$ are the corresponding quantities calculated as a function of variable cation fractions X_i and of the cation-oxygen distance (Lavina et al., 2002). There is good agreement between cations Mg(T)-, Fe^{2+}(T)- and Cr^{3+}(M)-oxygen distances adopted here and those determined by Lenaz et al. (2004) in the $MgCr_2O_4$–$FeCr_2O_4$ solid solution series. In addition, the model of Bosi et al. (2009) was adopted for electron hopping. During the minimisation process, Ni^{2+} and Ti^{4+} were fixed in the M site, due to their strong octahedral preference, whereas Si and Zn were fixed in the T site.

Table 4 lists the results for the seven new crystals (1A76-1C75), which are not significantly affected by previously reported cell parameter uncertainties. Table 4 also lists the cation distributions calculated for CROM1 as well as for magnetites the single crystal data of which are reported in Rossetti et al. (2009).

Some interesting features appear in the cation distribution of Table 4, where samples are ordered according to the transformation from chromite to magnetite. CROM1 shows the highest Cr (up to 1.4 a.f.u.) and Al (up to 0.5 a.f.u.) contents, with composition nearest to the original chromite. In fact, Mg is fully ordered in T site only in CROM1, meaning 'normal' structure; consequently, it is definitely out of the hopping zone. This is also supported by the Fe^{2+} and Fe^{3+} contents, partially ordered in T and M sites, respectively, although Fe^{3+}(T), about one-third that of the total tetrahedral ions, is still considerable. It should be recalled that, in CROM1, the thin volume of magnetite overgrowth (Figure 1) does not affect X-ray diffraction, since we only obtained a cation distribution typical of a normal structure. During this study, we were unable to find other samples with the same features.

In fact, Cr-magnetite 1A76, with average Cr content of 0.7 a.f.u., already shows an inverse structure. Note that:

Table 4. Cation distribution in CROM1, Cr-magnetites and magnetites.

	CROM1 U	1A76	1A74	1D55	3D45	1C74	1B74	1C75	LG12	LG10	LG52 V	LG22 C	LG45	LG47	LG49
T site															
Al	0.001	0.001	0.001	0.000	0.000	0.000	0.000	0.000	0.000	0.000	0.000	0.000	0.000	0.000	0.000
Fe^{2+}	0.518	0.330	0.191	0.138	0.133	0.110	0.121	0.067	0.040	0.054	0.058	0.071	0.068	0.066	0.058
Fe^{3+}	0.324	0.642	0.793	0.853	0.862	0.885	0.875	0.928	0.960	0.944	0.939	0.926	0.930	0.934	0.931
Mg	0.103	0.018	0.009	0.001	0.000	0.000	0.000	0.000	0.000	0.000	0.003	0.000	0.002	0.001	0.011
Mn^{2+}	0.034	0.000	0.001	0.003	0.000	0.000	0.001	0.001	0.000	0.002	0.000	0.003	0.000	0.000	0.000
Si	0.004	0.002	0.002	0.003	0.003	0.004	0.002	0.002	0.000	0.000	0.000	0.000	0.000	0.000	0.000
Zn	0.016	0.007	0.003	0.002	0.002	0.002	0.001	0.002	0.000	0.000	0.000	0.000	0.000	0.000	0.000
Sum	1.000	1.000	1.000	1.000	1.000	1.000	1.000	1.000	1.000	1.000	1.000	1.000	1.000	1.000	1.000
M site															
Al	0.084	0.006	0.004	0.002	0.003	0.002	0.002	0.002	0.000	0.000	0.000	0.000	0.005	0.003	0.000
Fe^{2+}	0.323	0.574	0.739	0.818	0.817	0.846	0.841	0.897	0.919	0.902	0.876	0.822	0.792	0.840	0.787
Fe^{3+}	0.573	0.617	0.814	0.846	0.862	0.908	0.943	0.957	0.996	1.026	1.057	1.073	1.063	1.062	1.066
Mg	0.006	0.046	0.042	0.036	0.042	0.040	0.035	0.033	0.038	0.042	0.052	0.097	0.123	0.084	0.139
Cr^{3+}	0.999	0.703	0.362	0.273	0.249	0.184	0.160	0.098	0.032	0.018	0.002	0.000	0.000	0.000	0.000
Ti^{4+}	0.005	0.014	0.010	0.009	0.008	0.007	0.007	0.006	0.006	0.006	0.001	0.000	0.000	0.000	0.000
Mn^{2+}	0.008	0.038	0.025	0.012	0.014	0.009	0.007	0.004	0.004	0.003	0.011	0.008	0.019	0.012	0.009
Ni^{2+}	0.002	0.004	0.004	0.005	0.005	0.005	0.004	0.004	0.005	0.004	0.002	0.000	0.000	0.000	0.000
Sum	2.000	2.000	2.000	2.001	2.001	2.000	2.000	2.000	2.000	2.000	2.000	2.000	2.001	2.001	2.001
FCN	1.76	1.16	0.74	1.28	1.44	4.65	4.69	0.81	0.18	0.55	0.16	0.69	1.27	1.40	3.18
f.v.	(*)	2.52	2.52	2.51	2.51	2.52	2.53	2.51	2.52	2.53	2.55	2.57	2.57	2.56	2.58

U: Ussel (from CROM1 to LG10), V: Valmeriana, C: Cogne (from LG22 to LG49).
FCN: residuals after minimisation process.
f.v.: Fe(M) formal valence.
(*) out of the hopping zone.

- its mean composition closely approaches that hypothesized at the chromite-magnetite boundary, and its Ti^{4+} content is the highest among all samples (Tables 1 and 4);
- the cell dimension and refined structural parameters have the largest standard deviations (Table 3).

Mg begins to order in M site and Fe^{2+} and Fe^{3+} begin to order opposite CROM1. However, Fe^{2+}(T) content is still about one-third that of the total tetrahedral ions.

With Cr content less than 0.4 a.f.u. (1A74), Mg is almost completely ordered in M site; Fe^{2+} becomes increasingly ordered in M site. Progressive Cr depletion to about 0.10 a.f.u. (1C75) is responsible for full ordering of Mg in M site and further increase in Fe^{2+}(M), but without reaching the fully 'inverted' structure, given the appreciable amounts of Fe^{2+} in T site.

Table 4 continues with the cation distribution of the magnetites representative of the whole study area. Magnetites from Ussel (LG12, LG10) and Valmeriana (LG52) represent a further stage of Cr depletion, with Cr reduced to 0.03, 0.02 a.f.u. (Ussel) and to mere traces (Valmeriana); they show similar behaviour to that of the previous

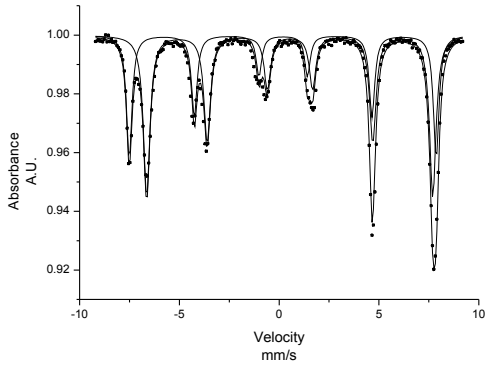

Figure 6. Mössbauer effect spectrum obtained at R.T. for sample LG12.

1C75, with still appreciable amounts of Fe^{2+} in T site. In the magnetites from Cogne (LG22, 45, 47, 49) Cr was not detected, and nor were Ni or Ti. Divalent iron is substituted by Mg up to 0.14 a.f.u., and also by minor amounts of Mn, whereas Fe^{3+} is very close to the ideal content of 2-3 spinels (2 a.f.u.). The Cogne magnetites fit the magnetite-magnesioferrite join; the Fe^{2+} content is definitely the lowest in the Aosta Valley samples. As in magnesioferrite, Mg is ordered in M site (O'Neill et al., 1992; Lenaz et al., 2006) and a definite amount of Fe^{2+} remains in T site, as in all the other samples studied.

Mössbauer spectroscopy

LG12 spectrum is typical of a substituted magnetite, that is with iron partially replaced by other divalent and trivalent cations, and consists of two partially overlapping sextets (Figure 6). The differences between this spectrum and that reported for pure magnetite are small, but significant (Table 5). Concerning Fe^{3+} in T site, there is a slight increase in the δ value (from 0.27 to 0.30 mm/s) and in the % area, whereas H_{int} decreases from 49.18 to 47.68. In the same way, the parameters for $Fe^{2.5+}$ in M site show a similar trend, except for the % area, which clearly decreases from 67% to 61%. Variations in the

Table 5. Mössbauer parameters for sample LG12.

	δ	$^{2\varepsilon}$Q	H_{int}	Γ	A	attribution
LG12	0.302	-0.023	47.68	0.33	39	Fe^{3+}(T)
	0.648	-0.012	44.45	0.39	61	$Fe^{2.5+}$ (M)
Ref. a	0.266	<0.025	49.18	b	33	Fe^{3+} (T)
	0.665	<0.025	46.07	c	67	$Fe^{2.5+}$ (M)

Ref a: Vandenberghe and De Grave (1989).
b, c: $Fe^{2.5+}$ (M) presents a linewidth considerably larger than Fe^{3+} (T).

isomer shift and internal field may be due to changes in the Curie points with composition (Robbins et al., 1971) or to different redistributions of the 3d electron shell, again induced by substitution (Russo et al., 2005). The differences in the % area for M and T sites may be due to the Cr for Fe substitution in M; in this

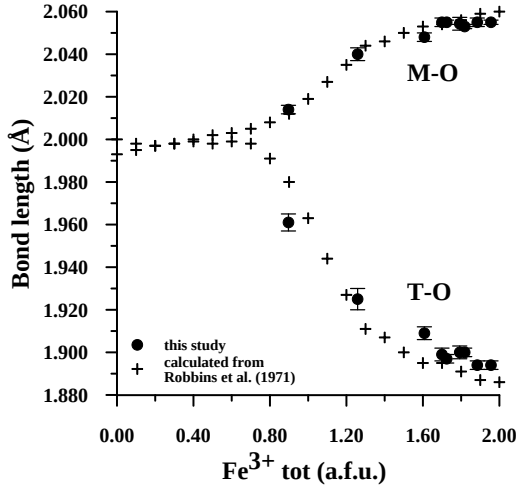

Figure 7. Plot of M-O and T-O bond lengths (Å) against Fe^{3+} tot (a.f.u.) in Cr-magnetites and CROM1. Also plotted are values calculated for synthetic system (Robbins et al., 1971) (see text). T-O bond lengths in Cr-magnetites tend to be slightly longer than those of synthetic samples, unlike CROM1.

Table 6. Cation distribution and structural parameters, calculated from data of Robbins et al. (1971).

Fe^{3+} tot	Fe^{3+}(M)	Fe^{2+}(M)	Fe^{2+}(T)	a [1] (Å)	a[2] (Å)	a calc. (Å)	u calc.	T-O (Å)	M-O (Å)
0.0	0.000	0.000	1.000	8.378	8.377	8.378	0.2628	2.000	1.993
0.1	0.080	0.020	0.980	8.382		8.382	0.2627	1.999	1.995
0.2	0.160	0.040	0.960	8.387	8.385	8.385	0.2625	1.997	1.997
0.3	0.260	0.041	0.960	8.391	8.391	8.390	0.2625	1.998	1.998
0.4	0.357	0.043	0.957	8.396	8.395	8.396	0.2624	1.998	2.000
0.5	0.448	0.053	0.948	8.400		8.400	0.2624	1.999	2.001
0.6	0.541	0.059	0.941	8.406	8.404	8.405	0.2623	1.999	2.003
0.7	0.629	0.071	0.929	8.409	8.406	8.409	0.2622	1.998	2.005
0.8	0.670	0.130	0.870	8.407	8.405	8.407	0.2617	1.991	2.008
0.9	0.683	0.217	0.783	8.403		8.403	0.2611	1.981	2.012
1.0	0.645	0.355	0.645	8.396		8.396	0.2600	1.963	2.019
1.1	0.602	0.498	0.502	8.391		8.391	0.2588	1.945	2.027
1.2	0.568	0.632	0.368	8.388	8.388	8.388	0.2576	1.926	2.035
1.3	0.540	0.760	0.240	8.385		8.388	0.2565	1.911	2.044
1.4	0.601	0.799	0.201	8.384	8.388	8.389	0.2562	1.907	2.046
1.5	0.641	0.859	0.141	8.385		8.389	0.2557	1.900	2.050
1.6	0.702	0.898	0.102	8.387	8.388	8.390	0.2554	1.896	2.053
1.7	0.787	0.914	0.086	8.389		8.392	0.2553	1.895	2.054
1.8	0.854	0.946	0.054	8.392	8.392	8.393	0.2551	1.891	2.056
1.9	0.918	0.982	0.018	8.394	8.393	8.393	0.2548	1.887	2.059
2.0	1.000	1.000	0.000	8.395	8.396	8.395	0.2547	1.886	2.060

[1] Robbins et al. (1971).
[2] Francombe (1957).

way, the Fe^{3+} in excess with respect to that necessary for electron hopping gives rise to a sextet with parameters typical of octahedral Fe^{3+}. However, at least at room temperature, these are virtually identical to those of tetrahedral iron, and the sextet is so completely overlapped to that due to the already existing Fe^{3+} in T site.

The Mössbauer results are not in contrast with the cation distributions of Table 4, as the spectrum is still very similar to that of magnetite, and no trace of a normal spinel such as $FeCr_2O_4$ is evident. This is also consistent with the fact that, as previously stressed, we were not able to find any more grains like CROM1 with predominant normal structure.

Discussion

Comparison with synthetic systems

The studied Cr-magnetites have chemical compositions closely approaching 'region 3' of the $FeCr_2O_4$–$FeFe_2O_4$ join examined by Robbins et al. (1971). Quintiliani et al. (2011) recently synthesized spinel single crystals near 'region 1' of this join and studied them by Mössbauer spectroscopy. The only crystallographic datum supplied by Robbins et al. (1971) is the cell parameter, but since Cr occupies only M sites, the cation distributions and u parameters can easily be calculated according to Lavina et al. (2002) and Bosi et al. (2009) for the electron hopping process, which is fully effective in 'region 3'.

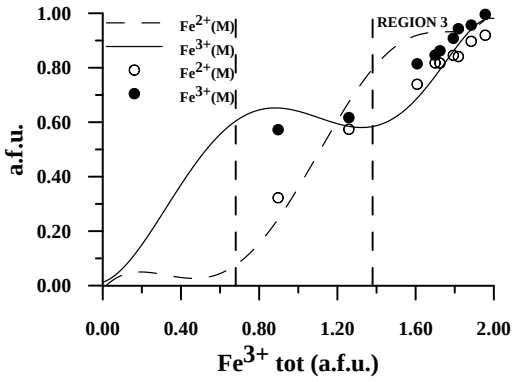

Figure 8. Plot of Fe^{2+}(M) (open circles) and Fe^{3+}(M) (filled circles) against Fe^{3+} tot (a.f.u.) in Cr-magnetites and CROM1. Dashed and continuous curves: 6th.-order polynomial best fit for Fe^{2+}(M) and Fe^{3+}(M), respectively, calculated for synthetic system (Robbins et al., 1971). Note in 'region 3': Fe^{3+}(M) > Fe^{2+}(M) in natural samples; vice versa in synthetic system.

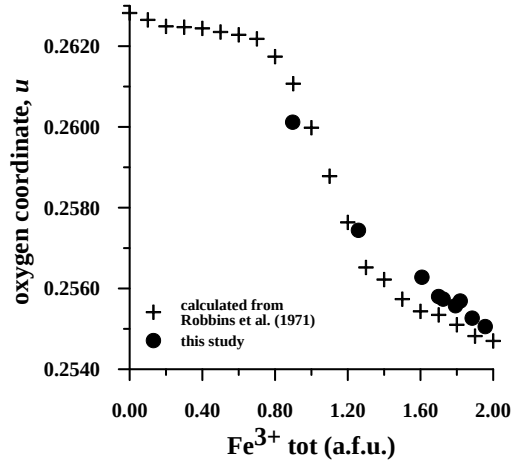

Figure 9. Plot of oxygen coordinate *u* against Fe^{3+} tot (a.f.u.); *u* values calculated after minimisation process from data of this study and from data of Robbins et al. (1971).

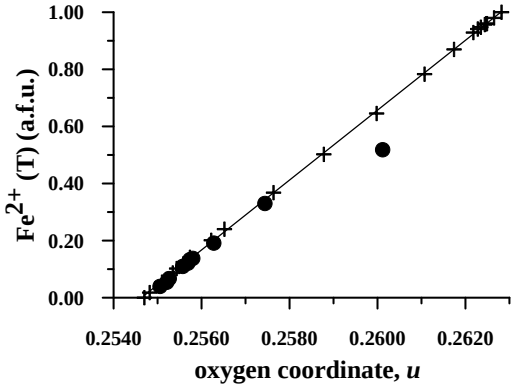

Figure 10. Straight-line correlation between Fe^{2+}(T) (a.f.u.) and oxygen coordinate *u* for Cr-magnetites and for Robbins et al. (1971) data. Symbols as in Figure 9. CROM1 plots off this trend, due to quite different population in T site.

Results are reported in Table 6 and shown in Figures 7, 8, 9 and 10.

According to our calculations, along this join, Cr displaces not only Fe^{3+} from M site, but also a definite amount of Fe^{2+}, maintaining Fe^{2+}(M) > Fe^{3+}(M) throughout 'region 3' (Figure 8). This result is not in contrast with the Mössbauer data by the above authors (Figure 9 in Robbins et al., 1971) and is consistent with the non-linearity of the *a* trend in their Figure 1 (reproduced in our Figure 2).

We note that, close to Fe^{3+} = 1.4 a.f.u., the *a* values determined by Robbins et al.(1971) are too small to be fitted with any iron distribution; instead, the higher values determined by Francombe (1957) are easily fitted (Figure 2). The low *a* values of Robbins et al. (1971) may be consistent with the presence of about 0.02 vacancies per 3.00 cations, a hypothesis which requires new experimental data.

Figure 10 shows the perfectly straight correlation between the *u* oxygen coordinate and the amount of Fe^{2+} disordered in T site, for both the synthetic samples and the Cr-magnetites

studied here. This again reveals the close similarity between them; in fact, CROM1, having quite a different population in T site, plots off this trend (see also Figure 2).

Iron distribution in natural Cr-magnetites and magnetites

As in the synthetic chromite-magnetite join, Cr is replaced by both Fe^{3+} and Fe^{2+} in M site, but the $Fe^{3+}(M)/Fe^{2+}(M)$ ratio is always greater than 1.0, unlike the synthetic samples (Table 4 and Figure 8). In all our Cr-magnetites covered by 'region 3' (including 1A76, which is at its limit), the formal valence of iron in M site is 2.51–2.53$^+$, very close to that of pure magnetite, 2.50$^+$.

The Fe(M) formal valence is slightly greater in the Cogne magnetites, where the total removal of Cr, Ti and Ni is accompanied by a significant increase in a divalent ion, Mg, up to 0.14 a.f.u.; definite disorder of Fe^{2+} in T site is still visible. However, note that, in this case, higher Mg(M) contents do not give higher $Fe^{2+}(T)$ contents (e.g., sample LG49); should this be the case, in fact, the Fe average valence in M site would increase significantly to well above 2.5$^+$. The previously described tendency always to retain an average formal iron valence near 2.5$^+$ on M site suggests that the charge hopping process may play a structure-stabilising role.

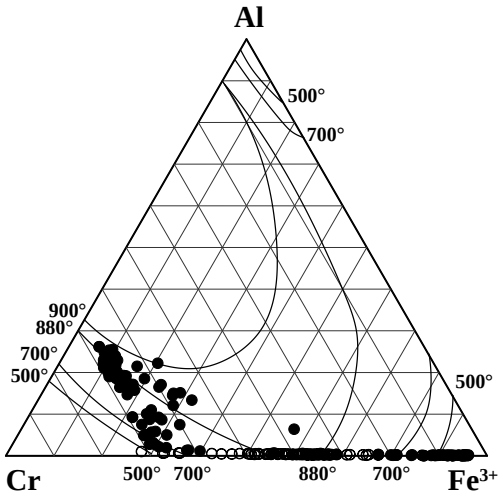

Figure 11. Ternary Fe^{3+}-Al-Cr plot for all analyses in CROM1 (solid circles) and all analyses in 1A76 (open circles). Also shown: approximate position of some solvi determined by Cremer (1969).

Conclusions

The studied samples are characterised by:
- replacement of Cr by both Fe^{2+} and Fe^{3+} in M site, all near 'region 3' of Robbins et al. (1971);
- the strong preference of Mg for the octahedral site, as in magnesioferrites and also the similar behaviour of Mn in Cr-poor samples, contrary to their ordering in T site (normal structure) in the Cr-rich sample CROM1;
- a definite inversion degree of Fe^{2+} in T site, even in the Cogne Cr-free magnetite; the small but significant Fe^{2+} content in T site, present in all samples, displaces a similar quantity of Fe^{3+} from T site to M site, in most cases making $Fe^{3+}(M) >$ 1.00 a.f.u. and in any case $Fe^{3+}(M) > Fe^{2+}(M)$. Hence, the formal valence of iron is > 2.5$^+$.

The Cogne samples should be the last stage of the chromite to magnetite transformation, with the sole survival of the inverse spinel structure. Instead, samples from all the other ore deposits including Ussel (from which LG12 sample comes) retain an appreciable amount of relict Cr-enriched areas, and represent a transitional situation, where both normal and inverse structures still coexist. This is shown in Figure 3 by the abrupt change in bulk chemistry at the boundary between an area with high Cr - and hence with normal structure - and another area with magnetite inverse structure; it is remarkable that both occur in the same single crystal, within a unique array of oxygen atoms.

The inhomogeneous chemical composition revealed at the micrometer scale seems to be the consequence of a complex transformation which allowed the survival of microsites the

compositions of which recall, but do not fit, those of a chromite proto-ore.

Notwithstanding the caution necessary in comparing natural data with the synthetic systems Fe-Cr-Al (e.g., Cremer, 1969), the spread of the spot analyses over a wide range of isothermal curves in Figure 11 is very large, up to temperatures which are completely incompatible with the Alpine evolution of the Aosta Valley. This again suggests a transformation in progress, quenched far from equilibrium.

Acknowledgements

We would like to thank Prof. A. Ferrario for kindly providing the samples, as well as for many enlightening discussions. We are particularly grateful to Prof. E.M. Piccirillo for his great help during the preparation of this work. Reflected light observations by Prof. P. Frizzo were greatly appreciated. Prof. F. Nestola generously assisted S.C. during cell parameter determinations. Dr. L. Peruzzo (CNR-IGG) provided the SEM photograph of CROM1. Raul Carampin (CNR-IGG) is thanked for his generous assistance with microprobe analyses. Prof. F. Princivalle, Dr. M. Quintiliani and two anonymous reviewers are kindly acknowledged for reviewing the manuscript. Ms. G. Walton revised the English text.

References

Angel R.J., Allan D.R., Miletich R. and Finger L.W. (1997) - The Use of Quartz as an Internal Pressure Standard in High-Pressure Crystallography. *Journal of Applied Crystallography*, 30, 461-466.

Angel R.J., Downs R.T. and Finger L.W. (2000) - High-temperature -High-Pressure Diffractometry. in "High-Temperature and High-Pressure Crystal Chemistry", Hazen R.M. and Downs R.T. eds., *Reviews in Mineralogy and Geochemistry*, Mineral. Soc. of America and Geochem. Soc., Washington, 41, 559-596.

Barnes S.J. (2000) - Chromite in komatiites, II. Modification during greenschist to mid-amphibolite facies metamorphism. *Journal of Petrology*, 41(3), 387-409.

Beeson M.H. and Jackson E.D. (1969) - Chemical composition of altered chromites from the Stillwater complex, Montana. *American Mineralogist*, 54, 1084-1100.

Bosi F., Hålenius U. and Skogby H. (2009) - Crystal chemistry of the magnetite-ulvöspinel series. *American Mineralogist*, 94, 181-189.

Cremer V. (1969) - Die Mischkristallbildung im System Chromit-Magnetit-Hercynit zwischen 1000° und 500°C. *Neues Jahrbuch für Mineralogie - Abhandlungen*, 111(2), 184-205.

Della Giusta A., Princivalle F. and Carbonin S. (1986) - Crystal chemistry of a suite of natural Cr-bearing spinels with $0.15 \leq Cr \leq 1.07$. *Neues Jahrbuch für Mineralogie - Abhandlungen*, 155, 319-330.

Della Giusta A., Princivalle F. and Carbonin S. (1987) - Crystal structure and cation distribution in some natural magnetites. *Mineralogy and Petrology*, 37, 315-321.

Diella V., Ferrario A. and Rossetti P. (1994) - The magnetite ore deposits of the southern Aosta Valley: chromite transformed during an Alpine metamorphic event. *Ofioliti*, 19(2a), 247-256.

Fontana E., Panseri M. and Tartarotti P. (2008) - Oceanic relict textures in the Mount Avic serpentinites, Western Alps. *Ofioliti*, 33(2), 105-118.

Francombe M.H. (1957) - Lattice changes in spinel-type iron chromites. *Journal of Physics and Chemistry of Solids*, 3(1/2), 37-43.

King H.E. and Finger L.W. (1979) - Diffracted beam crystal centering and its application to high pressure crystallography. *Journal of Applied Crystallography*, 12, 374-378.

Lavina B., Salviulo G. and Della Giusta A. (2002) - Cation distribution and structure modelling of spinel solid solutions. *Physics and Chemistry of Minerals*, 29, 10-18.

Lenaz D., Skogby H., Princivalle F. and Hålenius U. (2004) - Structural changes and valence states in the $MgCr_2O_4$–$FeCr_2O_4$ solid solution series. *Physics and Chemistry of Minerals*, 31, 633–642.

Lenaz D., Skogby H., Princivalle F. and Hålenius U. (2006) - The $MgCr_2O_4$–$MgFe_2O_4$ solid solution series: effects of octahedrally coordinated Fe^{3+} on T–O bond lengths. *Physics and Chemistry of Minerals*, 33, 465-474.

Loferski P.J. and Lipin B.R. (1983) - Exsolution in metamorphosed chromite from the Red Lodge

district, Montana. *American Mineralogist*, 68, 777-789.

Mellini M., Rumori C., and Viti C. (2005) - Hydrothermally reset magmatic spinels in retrograde serpentinites: formation of "ferritchromit" rims and chlorite aureoles. *Contributions to Mineralogy and Petrology*, 149, 266-275.

Nakagiri N., Manghnani M.H., Ming L.C. and Kimura S. (1986) - Crystal structure of magnetite under pressure. *Physics and Chemistry of Minerals*, 13, 238-244.

O'Neill H.St.C., Annersten H. and Virgo D. (1992) - The temperature dependence of the cation distribution in magnesioferrite ($MgFe_2O_4$) from powder XRD structural refinements and Mössbauer spectroscopy. *American Mineralogist*, 77, 725-740.

Onyeagocha A.C. (1974) - Alteration of chromite from the Twin Sisters dunite, Washington. *American Mineralogist*, 59, 608-612.

Quintiliani M., Andreozzi G.B. and Skogby H. (2011) - Synthesis and Mössbauer characterization of $Fe_{1+x}Cr_{2-x}O_4$ ($0 \leq x \leq 2/3$) spinel single crystals. *Periodico di Mineralogia*, 80(1), 39-55.

Ralph R.L. and Finger L.W. (1982) - A computer program for refinement crystal orientation matrix and lattice constants from diffractometer data with lattice symmetry constrains. *Journal of Applied Crystallography*, 15, 537-539.

Robbins M., Wertheim G.K., Sherwood R.C. and Buchanan D.N.E. (1971) - Magnetic properties and site distributions in the system $FeCr_2O_4$ – Fe_3O_4 ($Fe^{2+}Cr_{2-x}Fe_x^{3+}O_4$). *Journal of Physics and Chemistry of Solids*, 32, 717-729.

Rossetti P., Gatta G.D., Diella V., Carbonin S., Della Giusta A. and Ferrario A. (2009) - The magnetite ore districts of the southern Aosta Valley (Western Alps, Italy): a mineralogical study of metasomatized chromite ore. *Mineralogical Magazine*, 73(5), 737-751.

Russo U., Nodari L., Faticanti M., Kuncser V. and Filoti G. (2005) - Local interactions and electronic phenomena in substituted $LaFeO_3$ perovskite. *Solid state Ionics*, 176, 97-102.

Salviulo G., Carbonin S. and Della Giusta A. (2000) - Powder and single-crystal X-ray structure refinements on a natural chromite: dependence of site occupancies on experimental strategies. *Materials Science Forum*, Vols. 321-324, 46-52.

Sheldrick G.M. (1997) - SHELXL-97, a program for crystal structure refinement. University of Göttingen, Germany.

Vandenberghe R.E. and De Grave E. (1989) - Mössbauer effect studies of oxidic spinels. In "Mössbauer spectroscopy applied to inorganic chemistry" Long G.J. and Grandjean F. Eds., Plenum Press, New York, Vol. 3, 59-182.

Zakrzevski M.A. (1989) - Chromian spinels from Kuså, Bergslagen, Sweden. *American Mineralogist*, 74, 448-455.

Submitted, October 2010 - Accepted, January 2011